




Influence of La_2O_3 content on the structural, mechanical, and radiation-shielding properties of sodium fluoro lead barium borate glasses

A. F. Abd El-Rehim^{1,2} and Kh. S. Shaaban^{3,*} 

¹ Physics Department, Faculty of Science, King Khalid University, P.O. Box 9004, Abha 61413, Saudi Arabia

² Physics Department, Faculty of Education, Ain Shams University, Heliopolis, Roxy, P.O. Box 5101, Cairo 11771, Egypt

³ Chemistry Department, Faculty of Science, Al-Azhar University, P.O. 71452, Assiut, Egypt

Received: 20 November 2020

Accepted: 27 December 2020

Published online:
23 January 2021

© The Author(s), under exclusive licence to Springer Science+Business Media, LLC part of Springer Nature 2021

ABSTRACT

The techniques of melt-quenching were used to manufacture $53\text{B}_2\text{O}_3\text{--}2\text{NaF--}27\text{PbO--}(20-x)\text{BaO--}x\text{La}_2\text{O}_3$ ($0 \leq x \leq 15$) glass system. To check the status of these samples, the XRD diffractometer procedure was used. The molar volume of the glass system is decreased while density is increased. The current glass sample's mechanical properties depend on the glass structure. Ultrasonic velocity and elastic modulus (experimental and theoretical) of glass samples were observed to be increased. FT-IR analysis shows that with the increase of La_2O_3 increases the changes of BO_3 to BO_4 and increases the degree of glass connectivity and the structural units of $(\text{BO}_3/2\text{F})^-$ tetrahedra are formed. It has been noted that the MAC values of glass samples are decreased to 1 meV, apart from a small increase at 0.1 meV. At low energy, this significant decline and small peak are directly linked to the current photoelectric effect. The sample with the highest La_2O_3 content is owned the MAC's greatest values. It has been noted that the (HVL) and (TVL) increase with the increase in the photon energy and La_2O_3 content rendering to the achieved results. It has been noted that the Z_{eff} has the largest values at lower energy and at lowering concentration of La_2O_3 content. It has been noted that EABFs and EBFs have originally lower values at low energy levels, because the photoelectric effect dominates and BaO is replaced by La_2O_3 .

1 Introduction

For a long time, halide glasses like NaF have been known to us [1]. Such glasses are formed by simply quenching the method by moltening their halides.

These glasses are inherently hygroscopic and have low values of glass transition temperature, by reducing their applicability. Therefore, these glasses are doped with transition metal ions (TMi) and rare earth ions (REi) to increase the resistance of

Address correspondence to E-mail: khamies1078@yahoo.com

hygroscopic. The halide glasses doped with (TMi) and (REi) have been more resistant to attack of hygroscopic [2]. To vary the properties of the glass like the dielectric, mechanical, thermal, and optical dopants with halides or sulphates are presented into the host glass [3]. Halides such as NaF and LiF are introduced to the glass matrix to generate mobile ion species Li^+ , Na^+ , etc. Several studies have shown that dopant halides do not enter the glass's macromolecular chain. Thus, halide glasses are great metal ion solvents. Due to its unique physical properties, glasses incorporating halide ions have long been studied. The development of numerous devices and technologies, including solid-state batteries and radiation protection, has led to investigations of such glasses [1–7]. Increasing attention has been devoted to fluoride-based glasses due to their potential use for making infrared optical components and fibres. Interesting and remarkable properties were demonstrated by the modified dimension of fluoroborate glasses synthesized by replacing some oxygen ions with fluoride ions [8–11].

Borate glasses can be regarded as an adaptable type of glass that is used in various applications because they have high thermal stability and optical properties. Besides, it is considered good for TMi, REi, and halides as host glasses. Due to their attractive structural, optical properties and infrared radiation shielding, there has been considerable interest in the study of borate-based glasses over the last few years [12–19]. Many efforts have been made to doping with lanthanide ions the lead fluoroborate glass, the result showing that this material is a good candidate for laser applications [20].

B_2O_3 –NaF–PbO–BaO glasses have also great attention and La_2O_3 to investigate their optical properties. FT-IR measurements of these glasses showed that tetrahedral fluoroborate (BO_3F) groups have the same characteristics as tetrahedral borate (BO_4) groups [21]. Because of their properties, these glasses are of benefit to optoelectronic devices: a high refractive index of about 2.2 and good physical and chemical stability. Studies of B_2O_3 –NaF–PbO–BaO doped with La_2O_3 are presented. In addition to Phy-X/PSD [22] software calculations, results from FT-IR, mechanical, and radiation are presented.

2 Experimental approaches

$53\text{B}_2\text{O}_3$ – 2NaF – 27PbO – $(20-x)\text{BaO}$ – $x\text{La}_2\text{O}_3$ ($0 \leq x \leq 15$) glasses in Table 1 have been prepared according to the chemical equation:

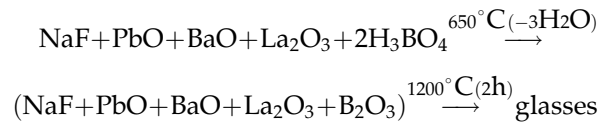


Table 1 annealed at 400°C glass samples. Glasses are prepared using the technique of melting/annealing.

A Rigaku Miniflex 600 X-ray diffractometer was used to test the glass states. Changes in the structure of these glasses will be explored by Bruker's VERTEX 70 FT-IR Spectrometers. Physical features of these glasses are projected as ion concentration of La^{3+} has been considered as

$$\text{Ti} = \left(\frac{6.023 \times 10^{23} x \text{ mol fraction of cation} \times \text{valency of cation}}{V_m} \right) \quad (1)$$

Inter-ionic distance (R_i) between La and La has been calculated as

$$R_i = \left(\frac{1}{\text{concentration of Ti}} \right)^{\frac{1}{3}} \quad (2)$$

La–La separation was projected as

$$(d\text{La} - \text{La}) = \left(\frac{V_m^B}{N} \right)^{\frac{1}{3}} \quad (3)$$

and $V_m^B = \frac{V_m}{2(1-2X_n)}$. The polaron radius r_p , and inter-nuclear distance r_i have been calculated as

Table 1 Chemical composition of the prepared glasses (in mol%)

Samples name	Chemical compositions				
	B_2O_3	PbO	NaF	BaO	La_2O_3
G 1	53	25	2	20	0
G 2	53	25	2	17.5	2.5
G 3	53	25	2	15	5
G 4	53	25	2	10	10
G 5	53	25	2	7.5	12.5
G 6	53	25	2	5	15

$$r_p = \frac{1}{2} \left(\frac{\pi}{6N} \right)^{\frac{1}{3}} \tag{4}$$

$$r_i = \left(\frac{1}{N} \right)^{\frac{1}{3}}. \tag{5}$$

Pulse-echo technique was applied to calculate ultrasonic velocities at room temperature. In this technique, 4 MHz transducers are *x*-cut and *y*-cut. The glass ultrasonic velocities had a measuring uncertainty of ± 15 m/s. The density (ρ) of the combined glass samples was measured using the Archimedes method at room temperature. The elastic moduli have been projected as [23–26]. Longitudinal modulus,

$$L = \rho v_l^2, \tag{6}$$

Shear modulus,

$$G = \rho v_s^2, \tag{7}$$

Young’s modulus,

$$Y = (1 + \sigma)2G, \tag{7}$$

Bulk modulus,

$$K = L - \left(\frac{4}{3} \right) G \tag{8}$$

The theoretical calculation of the dissociation energy and packing density of the elastic module is: [27, 28]

$$V_i = \left(\frac{3\pi}{4} \right) NA \{ mR_m^3 + nR_i^3 \} \left(\frac{m^3}{mol} \right), \tag{9}$$

where R_m and R_i are Pauling radii of metal and oxygen. The elastic moduli,

$$L = K + \left(\frac{4}{3} \right) G, \tag{10}$$

$$G = (V_i^2 G_i) / (V_i)^{-1}, \tag{11}$$

Poisson’s ratio,

$$\sigma = \frac{1}{2} - \left(\frac{1}{7.2 * V_i} \right), \tag{12}$$

Microhardness,

$$H = \frac{(1 - 2\sigma)Y}{6(1 + \sigma)}, \tag{13}$$

Debye temperature,

$$\theta_D = \frac{h}{k} \left(\frac{9N}{4\pi V_m} \right)^{\frac{1}{3}} M_s. \tag{14}$$

Average of ultrasonic velocities,

$$M_s = \frac{1}{3} \left(\frac{2}{v_l^3} + \frac{1}{v_t^3} \right)^{\frac{1}{3}}, \tag{15}$$

Thermal expansion,

$$\alpha_{P=23.2(v_L-0.57457)}, \tag{16}$$

Oxygen molar volume,

$$V_o = \left(\frac{M}{\rho} \right) \left(\frac{1}{\sum x_i n_i} \right) \tag{16}$$

Oxygen packing density,

$$OPD = \left(\frac{1000C}{Vm} \right) \left(\frac{Mol}{L} \right). \tag{18}$$

Phy-X/PSD can calculate numerous shielding variables at any level of energy [22]. The law of Beer-Lambert is written as

$$\mu = - \frac{\ln \frac{I}{I_0}}{x}, \tag{19}$$

where the linear coefficient of attenuation is μ (cm^{-1}) I_0 and I , respectively. The mass attenuation coefficient MAC (μ/ρ) has been estimated as

$$\left(\frac{\mu}{\rho} \right) = \sum_i w_i \left(\frac{\mu}{\rho} \right)_i, \tag{20}$$

where ρ is the density of the material and the coefficient of attenuation of mass is (μ/ρ). The mean free path (MFP) was calculated as

$$MEP = \left(\frac{1}{\mu} \right), \tag{21}$$

It is possible to calculate the tenth (TVL) and half-value layer (HVL) as

$$TVL = \left(\frac{\ln 10}{\mu} \right), \tag{22}$$

$$HVL = \left(\frac{\ln 2}{\mu} \right). \tag{23}$$

Z_{eff} can be estimated as

$$Z_{\text{eff}} = \left(\frac{\sigma_a}{\sigma_e} \right) \quad (24)$$

where σ_a is the atomic cross-sections

$$\sigma_a \sigma_a = \sigma_m \frac{1}{\sum_i n_i} = \left(\frac{\mu}{\rho} \right)_{\text{target}} / N_A \sum_i \frac{w_i}{A_i} \quad (25)$$

and σ_e is the electronic cross-sections

$$\sigma_e = \frac{1}{N} \sum_i \left(\frac{\mu}{\rho} \right)_i \frac{f_i w A_i}{z_i}, \quad (25)$$

G-P fitting parameters were estimated as $P = \frac{P_1(\log Z_2 - \log Z_{\text{eq}}) + Z_2(\log Z_{\text{eq}} - \log Z_1)}{\log Z_2 - \log Z_1}$. G-P fitting parameters have been estimated as $P = \frac{P_1(\log Z_2 - \log Z_{\text{eq}}) + Z_2(\log Z_{\text{eq}} - \log Z_1)}{\log Z_2 - \log Z_1}$ where P_1 and P_2 are the G-P fitting parameters corresponding to the atomic numbers Z_1 and Z_2 , respectively. EABF and EBF have been estimated by using G-P fitting $B(E, X) = 1 + \frac{b-1}{K-1}(K^x - 1)$ for $K \neq 1$, $B(E, X) = 1 + (b-1)x$ $K = 1$ where $K(E, X) = cx^d + d \frac{\tanh(\frac{x}{d}) - \tanh(-2)}{1 - \tanh(-2)}$ for $x \leq 40$. where E is the photon energy, x is the penetration depth in mfp, and $K(E, X)$ is the dose-multiplicative factor.

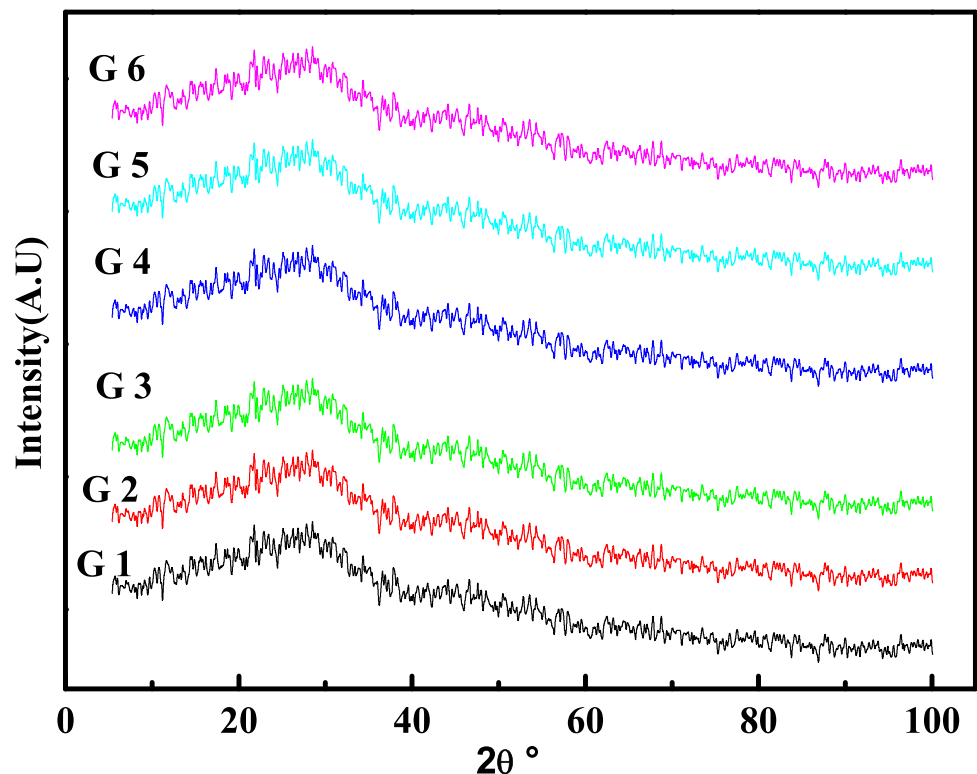
3 Results and discussions

3.1 Physical properties of glasses

Figure 1 shows the X-ray results of the studied glasses. These diffractograms show no discrete lines and no sharp peaks and indicate that the glass samples have a high degree of glassy state. The slight shift in the peak at (20–30) 2θ values with respect to La_2O_3 concentration can be related to the decrease in the bond length and to the higher coordination number with oxygen's.

Glass density is typically directly compared to molecular weights and densities [29–33]. In our paper, at the expense of BaO, La_2O_3 increased. The molecular weights of La_2O_3 and BaO [325.809 & 153.326] and densities [6.5 & 5.72 g/cm³] correspondingly. It has been observed that the density of our samples has increased. The increase in density is correlated to changes in the density and molecular weights of La_2O_3 and BaO. Due to the difference in atomic radii and bond length for Ba^{2+} and La^{3+} (0.4347 nm, 0.215 nm) and (0.3739 nm, 0.195 nm), respectively, the decrease in the molar volume of studied glasses. In Fig. 2, the density and molar volume are presented.

Fig. 1 XRD of the studied glasses



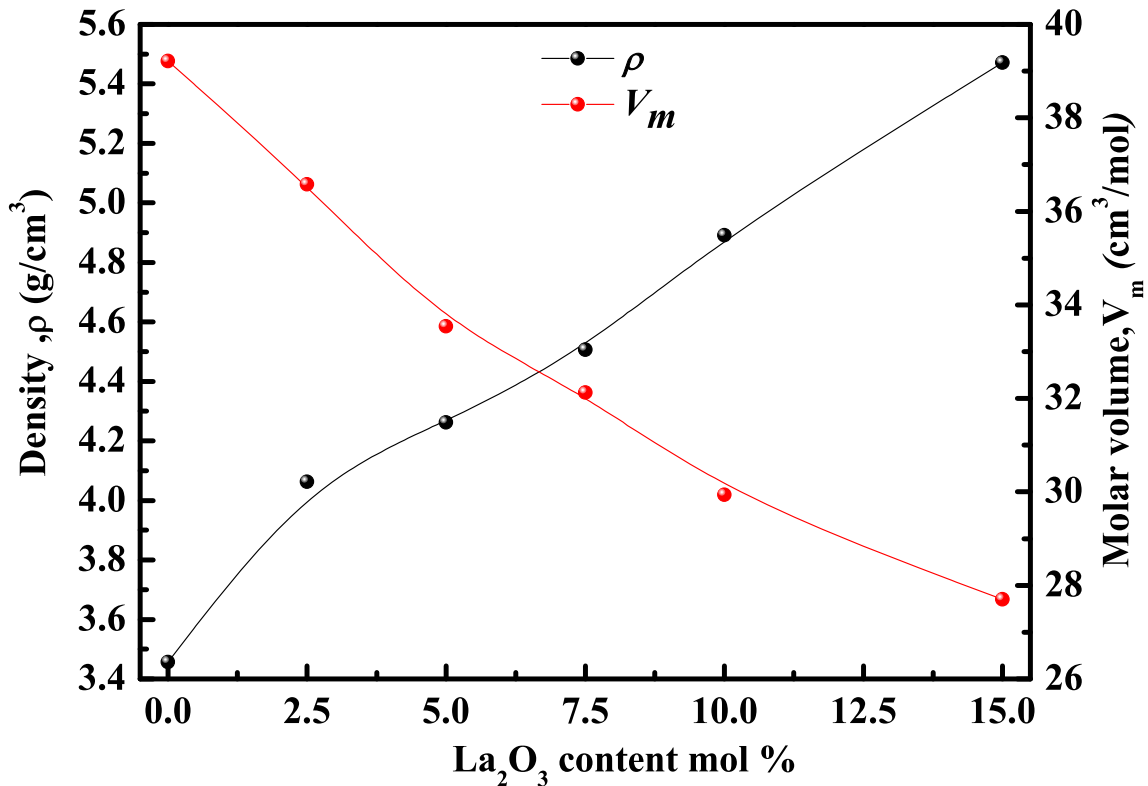


Fig. 2 Density and molar volume of the prepared samples with La₂O₃ by mol%

Table 2 Various physical parameters of the studied glasses

Samples	G 1	G 2	G 3	G 4	G 5	G 6
Ion conc. (<i>M_{oi}</i>) (10 ²¹ ions/cm ³)	–	1.43	2.9	4.46	6.26	9.89
Inter-ionic distance <i>R_i</i> (Å)	–	9.02	7.13	6.18	5.52	4.74
Inter-nuclear distance, <i>r_i</i> (Å)	–	10.44	8.265	7.173	6.415	5.515
Polaron radius, <i>r_p</i> (Å)	–	2.997	2.372	2.06	1.84	1.583
Boron–Boron separation(<i>d_{B–B}</i>), nm	0.558	0.531	0.523	0.515	0.502	0.484

Because of the reduction in molar volume, the concentration of La³⁺ has been raised. With the increase in La³⁺ concentration, the inter-ionic distance decreased, associated with decrease in molar volume. Because of the decrease in molar volume, values of (dLa–La) decreased with La₂O₃, as well as polaron radius, and inter-nuclear distance are decreasing. These values are shown in Table 2.

3.2 FT-IR analysis

The FT-IR spectrum of synthesised samples consisting of 6 perceptible vibrational absorption bands in the range of 400–4000 cm⁻¹ is illustrated in Fig. 3. The technique of deconvolution is used for resolving

wide bands [34–39]. Table 3 and Fig. 4 list the outcomes of the deconvolution process. It is therefore possible to the interpretation of the current FT-IR result obtained for B₂O₃–NaF–PbO–BaO–La₂O₃ glasses as follows: the first bands at ~ 3434 cm⁻¹, the second bands at ~ 1630 cm⁻¹, the third bands at ~ 1380 cm⁻¹, the fourth bands at ~ 995 cm⁻¹, the fifth bands at ~ 710 cm⁻¹, and the sixth bands at ~ 480 cm⁻¹. The band at ~ 3434 cm⁻¹ is accredited to vibrational modes of H₂O, OH, or BOH. The band at ~ 1630–1440 cm⁻¹ is accredited to the stretches of B–O in BO₃ (or BO₂O⁻) groups. The band at ~ 1088–830 cm⁻¹ is accredited to vibrations of tetrahedral BO₄ groups and B₂O₃ can be partially improved by NaF and the structural units of (BO₃/2

Fig. 3 Infrared spectra of the investigated glasses

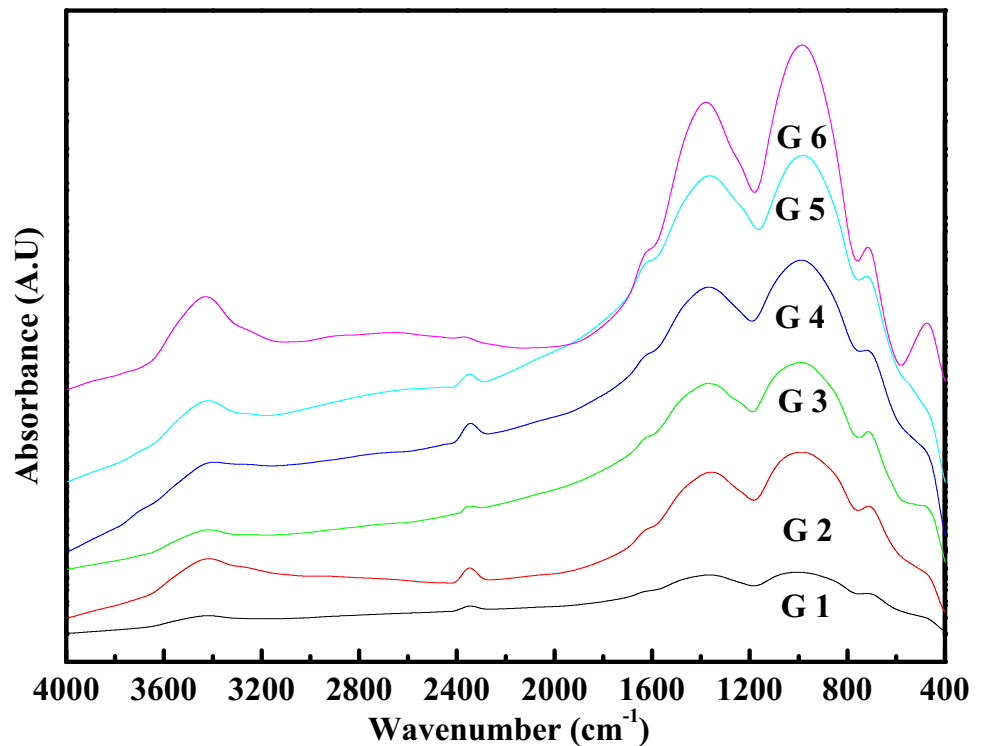


Table 3 The deconvolution parameter of the infrared spectra of studied glasses (C) is the component band centre, and (A) is the relative area (%) of the component band, the area under both (BO₄, BO₃) and N₄ fraction

												BO ₄	BO ₃	N ₄
G 1	C	468	579	–	701	850	963.5	1072	–	1321	1447			
	A	3.3	11.4	–	9.41	18.5	15.13	16.4	–	11.22	14.74	50.0123	25.9671	0.65823
G 2	C	463	564	–	703	830	952	1087	–	1316	1439			
	A	3.1	10.8	–	11.66	7.83	30.1	11.6	–	8.7	16.42	49.4533	25.094	0.66338
G 3	C	461	577	–	703	835	960	1092	–	1313	1450			
	A	5.41	10.6	–	9.5	12.82	21.9	14.44	–	9.9	15.6	49.1354	25.4369	0.6589
G 4	C	457	533	695	–	847	962	1088	–	1315	1443			
	A	3.54	10.5	16	–	11.89	21.4	13.93	–	8.9	13.9	47.1901	22.8023	0.67422
G 5	C	465	574	–	706	840	951	1065	1234	1342	1463			
	A	3.7	9.7	–	10.12	13.54	20.7	14.85	4.43	12.4	10.4	53.5492	27.2576	0.66268
G 6	C	479	–	665	709	847	963	1083	1237	1339	1453			
	A	4.7	–	4.3	4	15.96	19.84	19.86	6.45	11.8	13.2	62.0932	31.409	0.66408

F)[–] tetrahedra are formed. The band at $\sim 709\text{--}655\text{ cm}^{-1}$ is due to bending vibrations of B–O linkages in the borate units. The band at $\sim 579\text{--}463\text{ cm}^{-1}$ is accredited to Na⁺, Ba²⁺, Pb²⁺, and La³⁺.

In the fraction (N₄), the area under the bands was considered, $N_4 = \frac{BO_4}{(BO_4+BO_3)}$. As a result, the value of the N₄ fraction increases with the development

of structural units [BO₄]. In Table 4, peak assignments for the glass samples are provided. The addition of La₂O₃ increases the changes of BO₃ to BO₄ and increases the degree of glass connectivity.

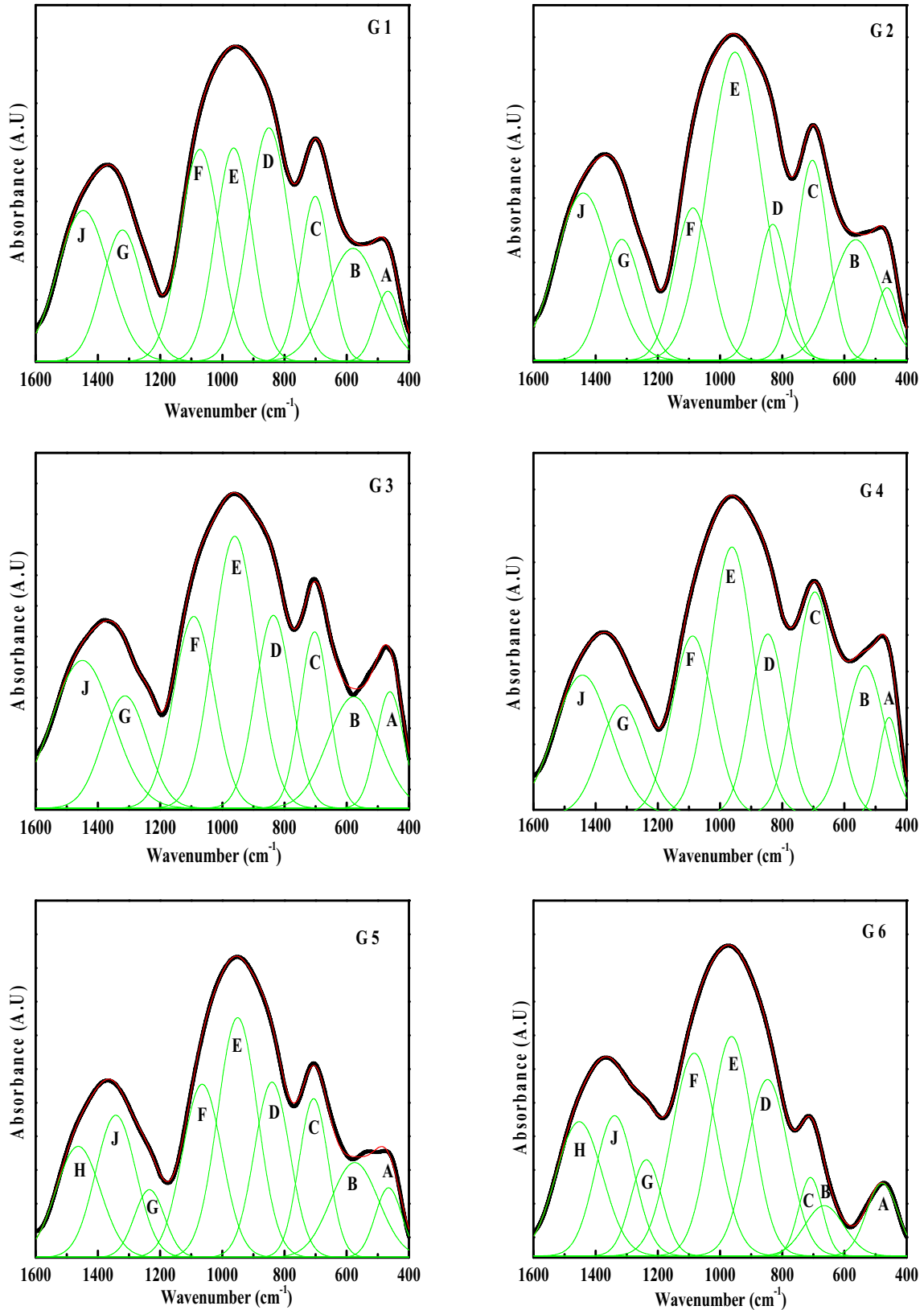
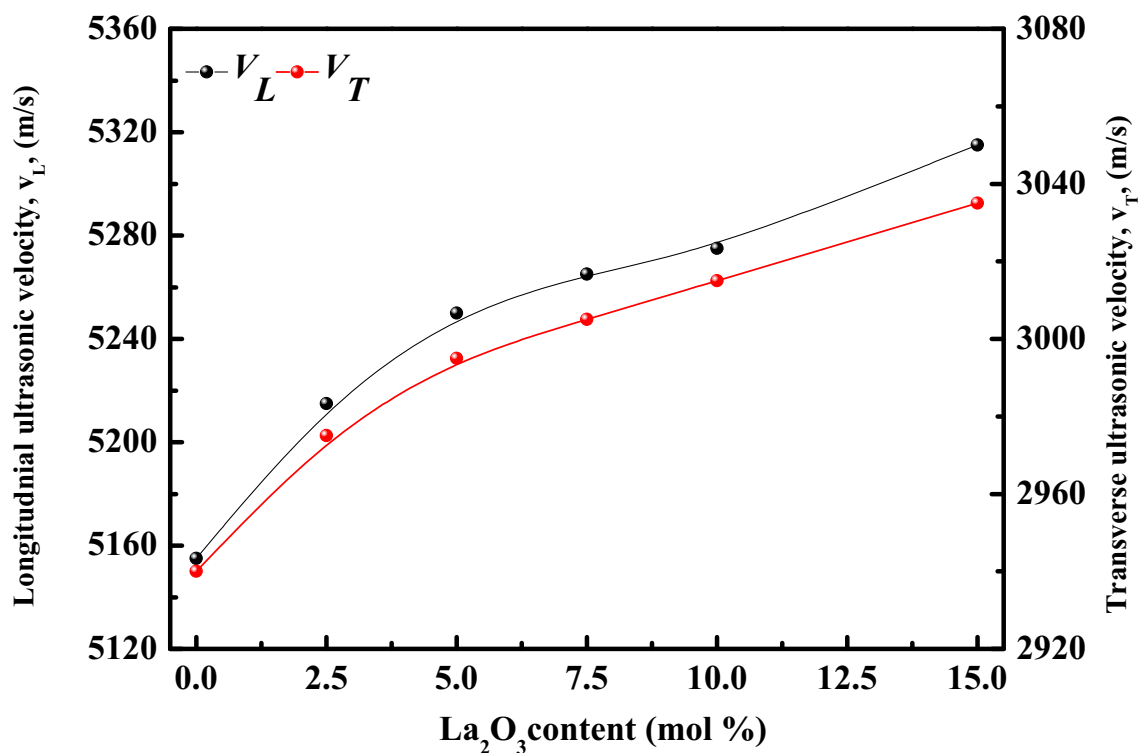


Fig. 4 Curve-fitting of IR spectra of the investigated glasses

Table 4 Peak assignments for the prepared glasses

Wavenumber, (cm ⁻¹)	Vibrational modes
~ 3434	Are accredited to vibrational modes of H ₂ O, OH or BOH
~ 1630–1440	Are accredited to the stretches of B–O in BO ₃ (or BO ₂ O ⁻) groups
~ 1088–830	Are accredited to vibrations of tetrahedral BO ₄ groups and B ₂ O ₃ can be partially improved NaF and the structural units of (BO _{3/2} F) ⁻ tetrahedra are formed
~ 709–655	Are due to bending vibrations of B–O linkages in the borate units
~ 579–463	Are accredited to Na ⁺ , Ba ²⁺ , Pb ²⁺ and La ³⁺

**Fig. 5** Dependence of the longitudinal and shear ultrasonic velocities v_L and v_T of the investigated glasses with La₂O₃ by mol%

3.3 Mechanical properties

Figure 5 and Table 5 represented sound velocities (V_L) and (V_T) of glasses. Both velocities have been observed to increase with the increase of La₂O₃ concentration. This observation because of increased density, cross-link density, and glass matrix connectivity. V_L increases from 5155 ms⁻¹ at 0% La₂O₃ to 5315 ms⁻¹ at 15% La₂O₃, and V_T increases from 2940 ms⁻¹ at 0% La₂O₃ to 3015 ms⁻¹ at 15% La₂O₃.

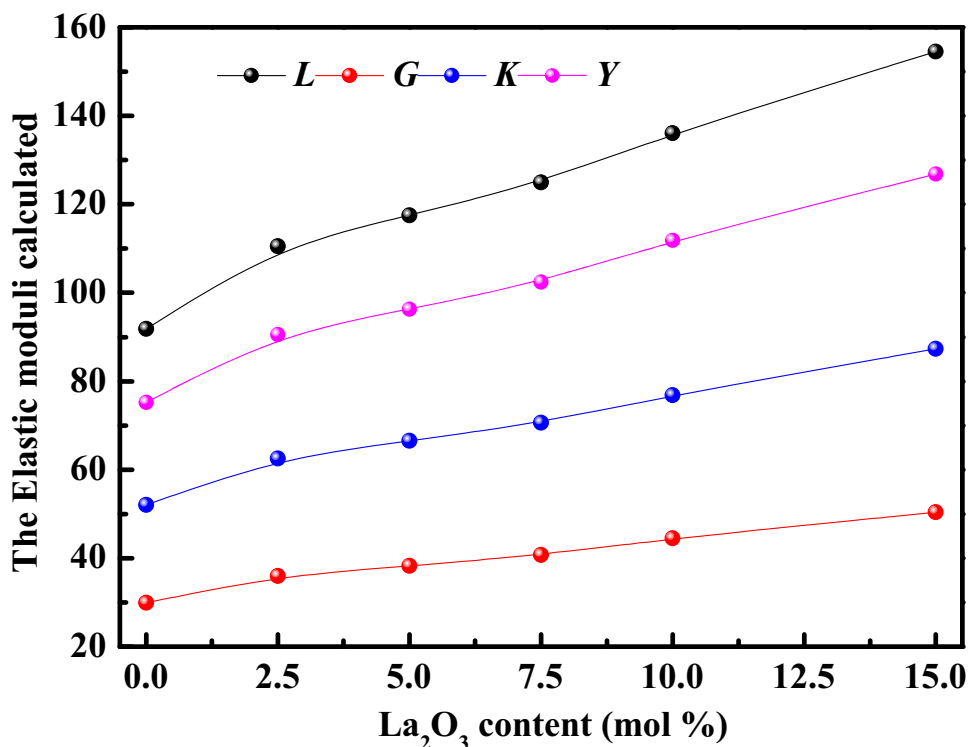
Based on the previous analysis of FT-IR, this conduct is associated with the increase in the N_4 and La–La separation. As well as the increase in (BO) and, consequently increased glass network connectivity, where the La breaks the bonds of BO₄ tetrahedral units with the structural units of (BO_{3/2} F)⁻ tetrahedra are formed.

Numerous types (experimental and theoretical) of elastic modules have been evaluated for the glass samples displayed in Figs. 6 and 7, and Table 6. Both

Table 5 The values of sound velocities and elastic moduli (experimental and theoretical) of the studied glasses

Samples name	v_L (m s ⁻¹)	v_T	L (GPa)	G (GPa)	K (GPa)	Y (GPa)	L_M (GPa)	G_M (GPa)	K_M (GPa)	Y_M (GPa)
G 1	5155	2940	91.84	29.87	52.01	75.22	52.2	21.29	23.81	46.62
G 2	5215	2975	110.5	35.96	62.54	90.52	59.7	23.03	28.99	51.76
G 3	5250	2995	117.5	38.23	66.5	96.26	70.21	25.31	36.47	58.42
G 4	5265	3005	124.92	40.69	70.66	102.42	77.95	26.94	42.03	63.09
G 5	5275	3015	136.1	44.46	76.81	111.81	90.18	29.33	51.08	69.97
G 6	5315	3035	154.51	50.39	87.36	126.8	110.4	33.1	66.3	80.66

Fig. 6 Elastic moduli calculated of the studied glasses with La₂O₃ by mol%



elastic modules have been observed to increase with the increase of La₂O₃ concentration. There is a clear link among elastic modules and ultrasonic velocity. This observation because of Ba–O bond strength is (33 kcal/mol) is lesser than La–O (58 kcal/mol) [40]. The increase of La₂O₃ causes a shift to higher wavenumbers which connected to the formation of BO₄ with the structural units of (BO_{3/2}F)⁻ tetrahedra are formed causes increase the connectivity of glass samples.

Other mechanical parameters such as (V_i), (G_i), (H), (α_P), (Z), (O_{PD}), (V_0), and (σ) are listed in Table 6. These parameters are affected by the glass network. All these parameters have been observed to increase with the increase of La₂O₃ concentration except

(V_0) as it is decreased because of the decrease in molar volume. This observation is in agreement with the analysis of FT-IR.

3.4 Radiation shielding properties

The degree of shielding in this paper was investigated from the increase of La₂O₃ at the expense of BaO with a nominal composition of 53B₂O₃–2NaF–27PbO–(20 – x) BaO– x La₂O₃ ($0 \leq x \leq 15$). First, the mass attenuation coefficients (MAC) is attained by Phy-X/PSD software calculations for the energy range of 0.015–15 meV to gather information about the resistance of the glass samples to ionizing radiation [30, 41–50]. The behaviour of the glass samples’ MAC values is exemplified in Fig. 8 based on the

Fig. 7 Elastic moduli theoretically of the studied glasses with La_2O_3 by mol%, according to Makishima–Mackenzie Model

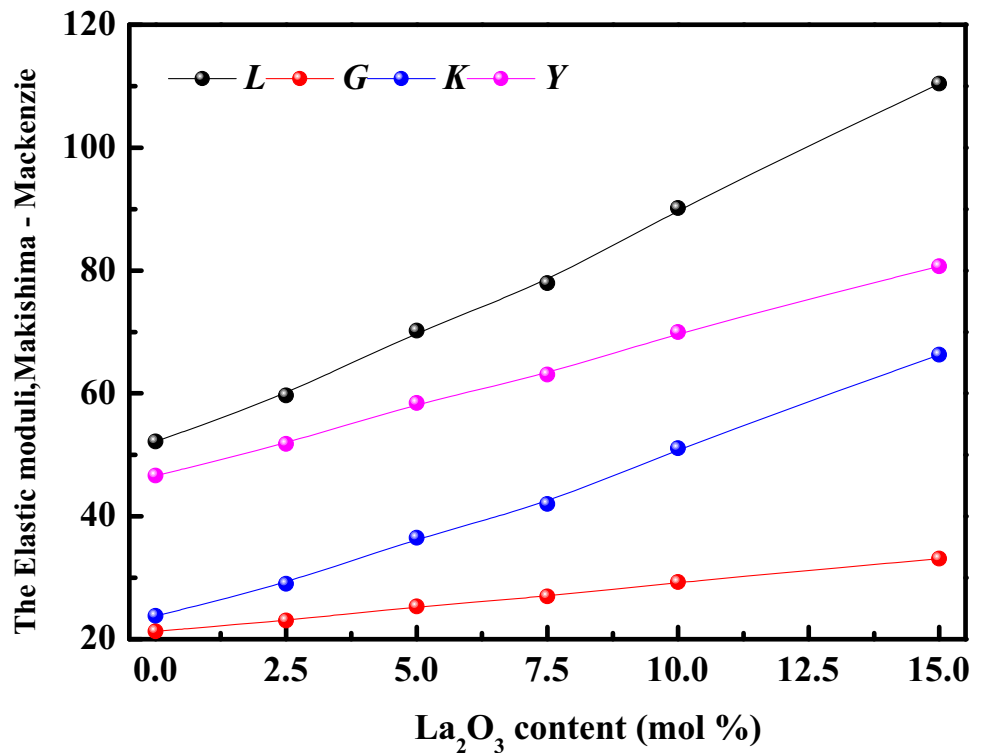


Table 6 Values of, packing density (V_i), dissociation energy (G_i), thermal expansion coefficient (α_p), acoustic impedance (Z), and Debye temperature (θ_D), oxygen packing density, oxygen molar volume (V_o), softening temperature (T_s), and microhardness (H) of glass systems

Samples name/parameters	$V_i \times 10^{-6}$, (m ³)	G_i , (kcal/kJ)	α_p , (K ⁻¹)	d	σ	$Z \times 10^7$ (kg.m ⁻² .s ⁻¹)	θ_D , (K)	O_{PD} , (mol/L)	V_o , (cm ³ /mol)	H , (GPa)	T_s , (°C)
G 1	0.43	13.1	119582.7	2.30	0.2	1.78	409.52	56.764	19.222	4.80	586.36
G 2	0.47	13.2	120974.7	2.30	0.2	2.12	422.64	66.067	17.501	5.78	646.96
G 3	0.52	13.4	121786.7	2.30	0.2	2.24	436.43	68.672	15.673	6.15	700.78
G 4	0.56	13.6	122134.7	2.30	0.3	2.37	442.67	71.963	14.667	6.55	749.86
G 5	0.61	13.7	122366.7	2.32	0.3	2.58	453.02	77.451	13.366	7.19	800.45
G 6	0.69	14	123294.7	2.31	0.3	2.91	464.65	85.301	11.838	8.13	906.36

energy of photons and La_2O_3 content. It has been noted that the MAC values of glass samples are decreased to 1 meV, apart from a small increase at 0.1 meV. This increase can be related to absorption edge of the atomic composition of the glasses. At low energy, this significant decline and small peak are directly linked to the current photoelectric effect. The sample with the highest La_2O_3 content is owned the MAC 's greatest values. This reduction is related to the molecular masses of BaO (153.326) with La_2O_3 (325.809) and density of samples. Therefore, the

addition of La_2O_3 leads to an increase of gamma-radiation protection. Figure 9 exemplified of LAC values based on the energy of photons and La_2O_3 content. It has been noted that the LAC values as MAC. Table 7 characterizes MAC (cm²/g) 53B₂O₃–2NaF–27PbO–5BaO–15La₂O₃ in comparison with other glasses.

The variations of the HVL and TVL values of the glasses based on the energy of photons are exemplified in Figs. 10 and 11. It has been noted that the (HVL) and (TVL) increase with the increase in the

Fig. 8 The mass attenuation coefficient (μ/ρ) of the investigated glasses versus the photon energy for the glasses

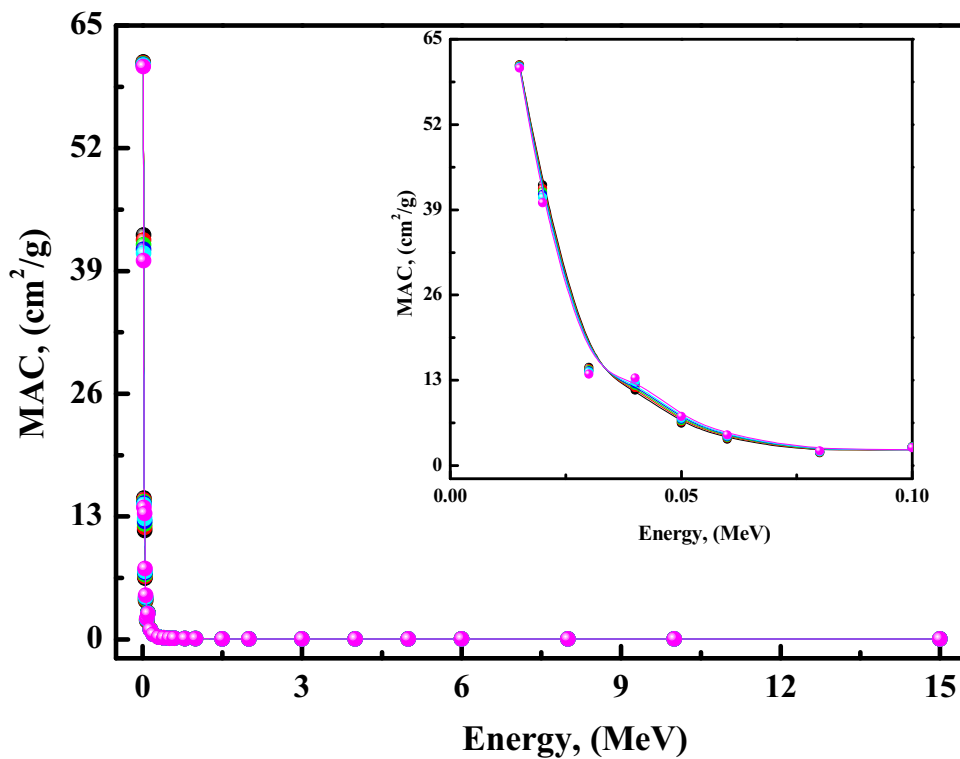


Fig. 9 Variation of linear attenuation coefficient (μ) values versus the photon energy for the glasses

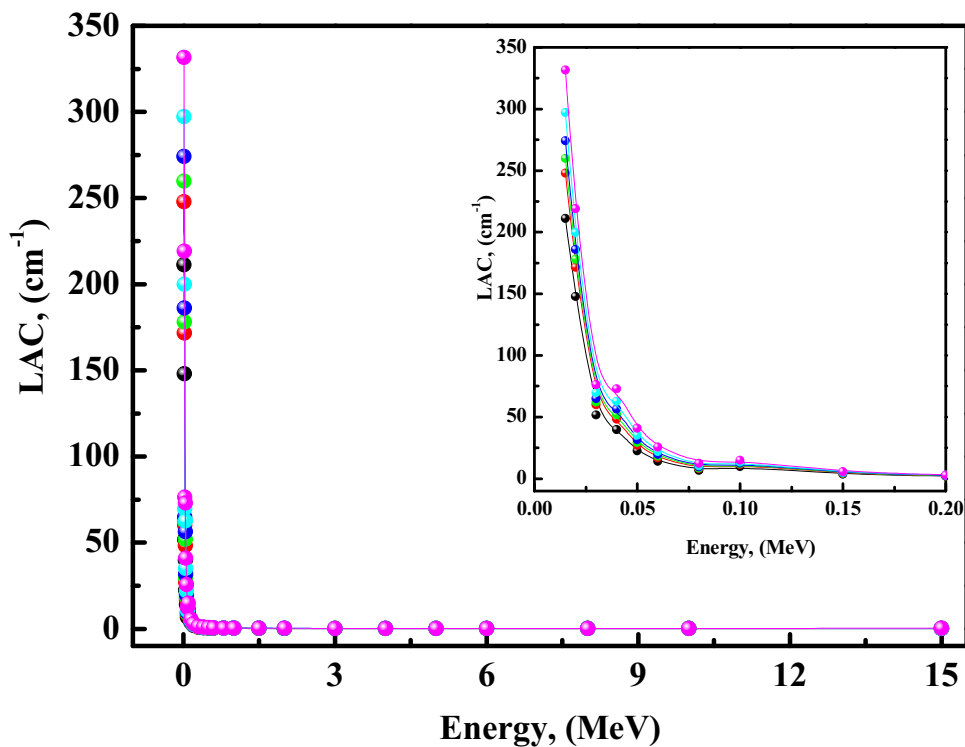
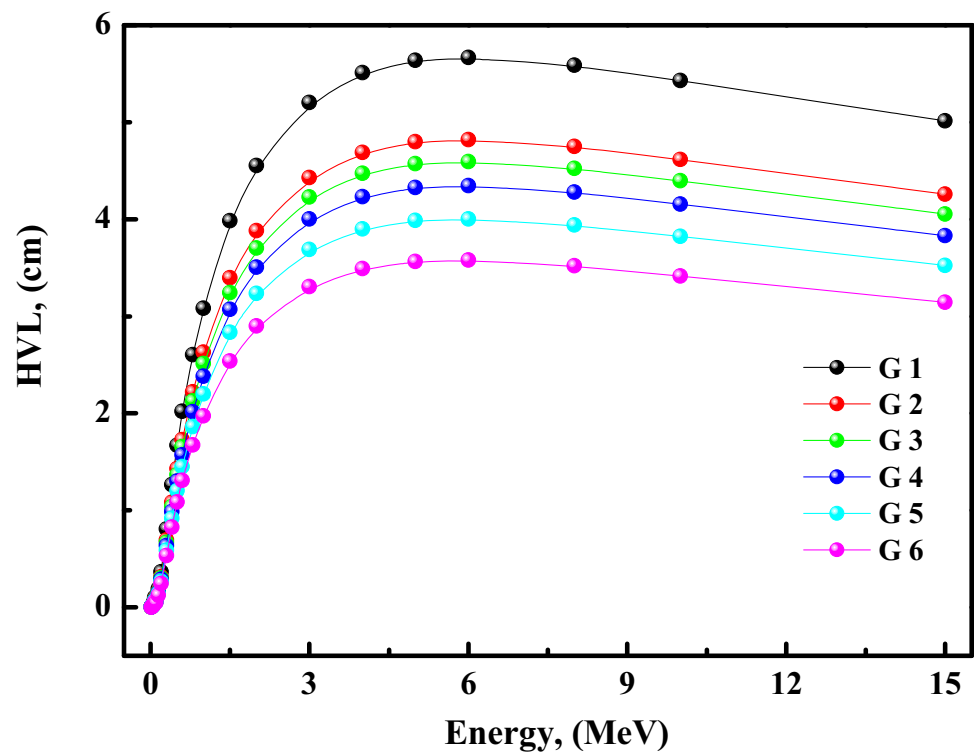


Table 7 Mass attenuation coefficients (in cm^2/g) of $53\text{B}_2\text{O}_3\text{-}2\text{NaF-}27\text{PbO-}5\text{BaO-}15\text{La}_2\text{O}_3$ in comparison with different glass samples

Samples	(MeV)	
	0.02	10
$53\text{B}_2\text{O}_3\text{-}2\text{NaF-}27\text{PbO-}5\text{BaO-}15\text{La}_2\text{O}_3$ [present work]	40.06405	0.0371
$66\text{B}_2\text{O}_3\text{-}5\text{Al}_2\text{O}_3\text{-}29\text{Na}_2\text{O}$	1.074	0.020
$5\text{Bi}_2\text{O}_3\text{-}61\text{B}_2\text{O}_3\text{-}5\text{Al}_2\text{O}_3\text{-}29\text{Na}_2\text{O}$	5.059	0.022
$10\text{Bi}_2\text{O}_3\text{-}56\text{B}_2\text{O}_3\text{-}5\text{Al}_2\text{O}_3\text{-}29\text{Na}_2\text{O}$	9.043	0.023
$0\text{PbO-}30\text{SiO}_2\text{-}46.67\text{B}_2\text{O}_3\text{-}23.33\text{Na}_2\text{O}$	1.386	0.023
$5\text{PbO-}25\text{SiO}_2\text{-}46.67\text{B}_2\text{O}_3\text{-}23.33\text{Na}_2\text{O}$	5.167	0.021
$10\text{PbO-}20\text{SiO}_2\text{-}46.67\text{B}_2\text{O}_3\text{-}23.33\text{Na}_2\text{O}$	8.952	0.024
$49.46\text{SiO}_2\text{-}26.38\text{Na}_2\text{O-}23.08\text{CaO-}1.07\text{P}_2\text{O}_5$	3.982	0.024
$47.84\text{SiO}_2\text{-}26.67\text{Na}_2\text{O-}23.33\text{CaO-}2.16\text{P}_2\text{O}_5$	3.985	0.023
$44.47\text{SiO}_2\text{-}27.26\text{Na}_2\text{O-}23.85\text{CaO-}4.42\text{P}_2\text{O}_5$	4.057	0.024
$40.96\text{SiO}_2\text{-}27.87\text{Na}_2\text{O-}24.39\text{CaO-}6.78\text{P}_2\text{O}_5$	4.113	0.024
$37.28\text{SiO}_2\text{-}28.52\text{Na}_2\text{O-}24.95\text{CaO-}9.25\text{P}_2\text{O}_5$	4.061	0.024
$48.98\text{SiO}_2\text{-}26.67\text{Na}_2\text{O-}23.33\text{CaO-}1.02\text{P}_2\text{O}_5$	3.983	0.023
$43.66\text{SiO}_2\text{-}28.12\text{Na}_2\text{O-}24.60\text{CaO-}3.62\text{P}_2\text{O}_5$	4.100	0.024
$38.14\text{SiO}_2\text{-}29.62\text{Na}_2\text{O-}25.91\text{CaO-}6.33\text{P}_2\text{O}_5$	4.190	0.022
$40.71\text{SiO}_2\text{-}28.91\text{Na}_2\text{O-}25.31\text{CaO-}5.07\text{P}_2\text{O}_5$	4.131	0.022

Fig. 10 The half-value layer for the prepared glasses as a function of photon energy



photon energy rendering to the achieved results. At low energy, the HVL of all samples is close together due to the increase of secondary scattering photons. These data reveal that the energy increase makes the photon capable of deliberately transmitting the

prepared sample. In the energy range of 12–15 meV, HVL values are reduced because of absorption and loss of energy during the PP process. The sample $53\text{B}_2\text{O}_3\text{-}2\text{NaF-}27\text{PbO-}5\text{BaO-}15\text{La}_2\text{O}_3$ has the lowest HVL and TVL values. Figure 12 exemplifies that

Fig. 11 The tenth value layer for the prepared glasses as a function of photon energy

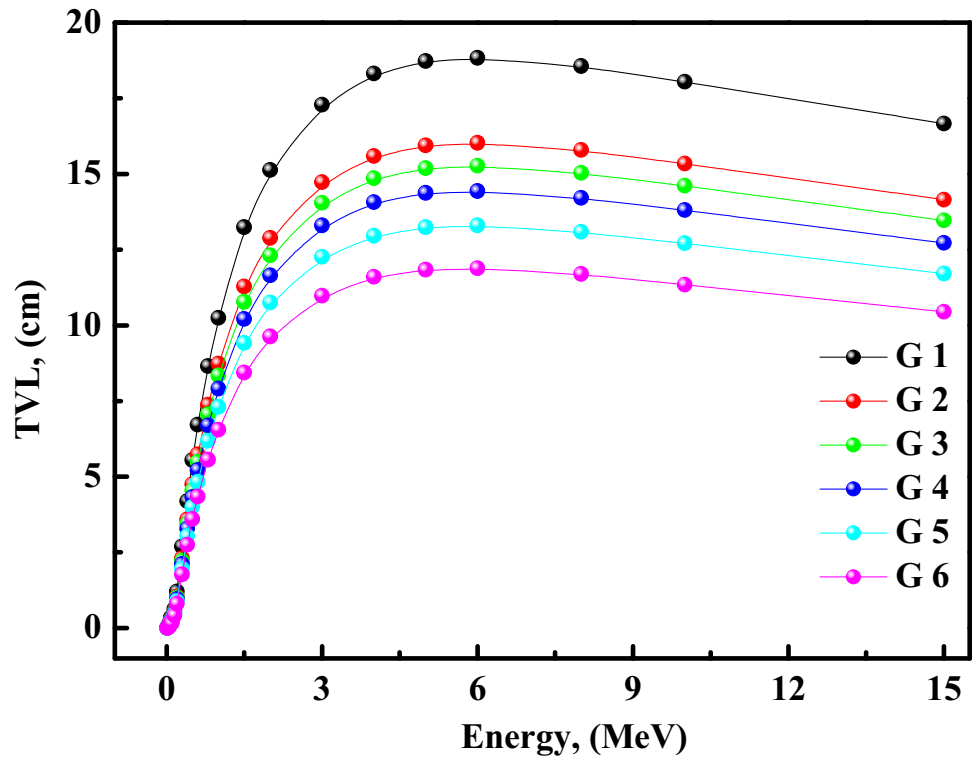


Fig. 12 The comparison of half-value layer for the prepared glasses as a function of photon energy with standard materials

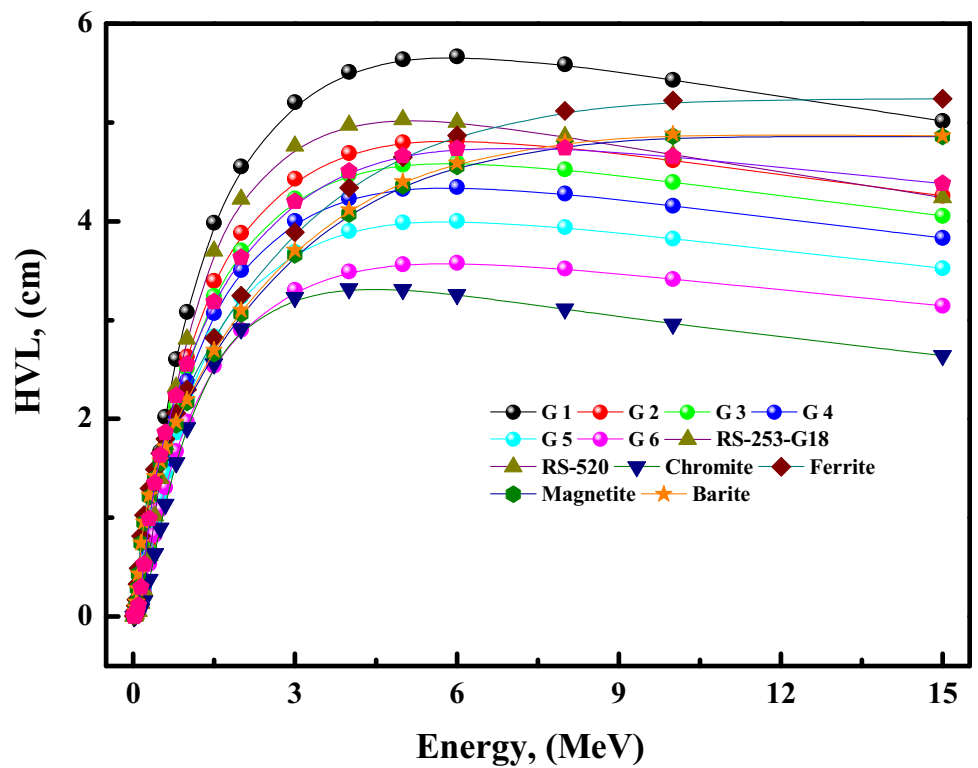
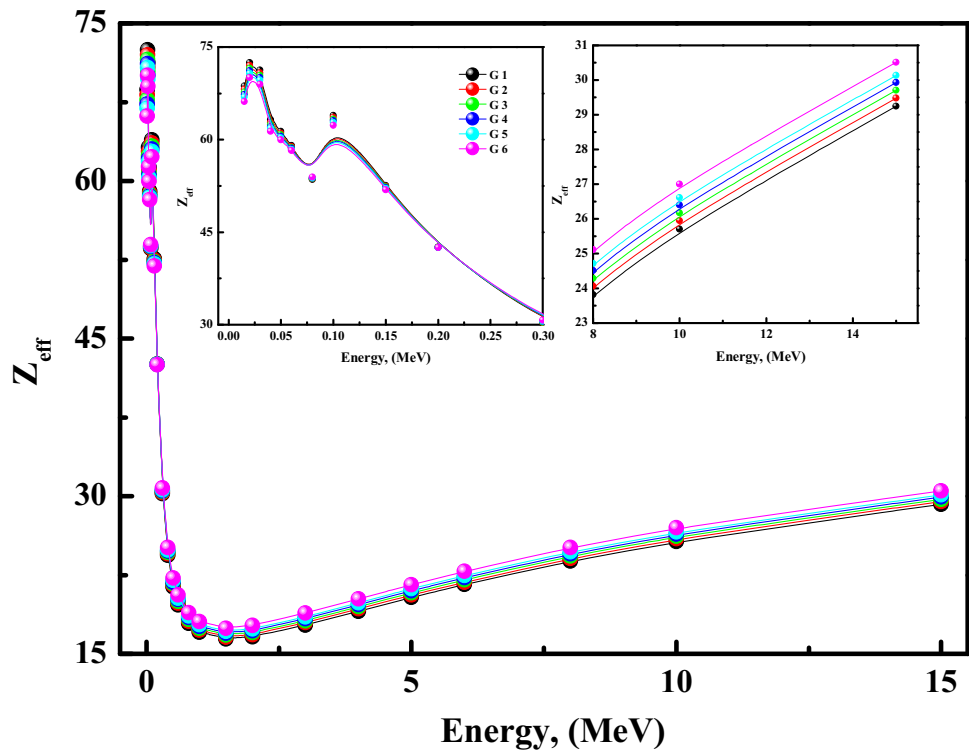


Fig. 13 Variation of effective atomic (Z_{eff}) number values as a function of photon energy for the glasses



HVL of examined glasses is compared with barite, magnetite, ferrite, chromite, RS-253-G18, and RS-520. HVL values of examined glasses are in the same range of predictable materials. The behaviour of TVL based on the energy of photons and La_2O_3 content is like HVL.

The variation of Z_{eff} based on the energy of photons and La_2O_3 content is exemplified in Fig. 13. It has been noted that the Z_{eff} has the largest values at lower energy and at lowering concentration of La_2O_3 content. The Z_{eff} values for samples decreased rapidly in the range of 0.05–0.1 meV and from G 1 to G3 because of photoelectric effect. There is a sudden growth in the energy range of 3–15 meV and from G3 to G 6 for all the glasses because of interaction of Compton scattering. The sample $53\text{B}_2\text{O}_3\text{--}2\text{NaF--}27\text{PbO--}5\text{BaO--}15\text{La}_2\text{O}_3$ has the highest values of Z_{eff} .

Both build-up factors EABF and EBF of glass samples based on the energy of photons are exemplified in Figs. 14 and 15. Tables 8 and 9 provide the G-P fitting parameters of the investigated glasses [30, 41–56]. It has been noted that at low energy

levels, the EABFs and EBFs originally possess very high values, as the photoelectric effect dominates and replaces the BaO with La_2O_3 . At 0.01–0.05 meV, it has been noted that there are very sharp bands for EABF and EAB. Clearly, by replacing BaO with La_2O_3 , the intensity of those increments is reduced because of the K absorption edges of La and Ba. At 0.2 meV, it has been noted that the values of EABF and EBF began to rise gradually because of the formation of secondary scatterings. The interaction of photons with matter atoms is more than that of air due to the greater atomic number of La and Ba in the glass composition. Therefore, for all samples, the EABF values are higher than the EBF as shown Figs. 14 and 15. In addition, the EABF and EBF values of $53\text{B}_2\text{O}_3\text{--}2\text{NaF--}27\text{PbO--}5\text{BaO--}15\text{La}_2\text{O}_3$ are lower than the other samples.

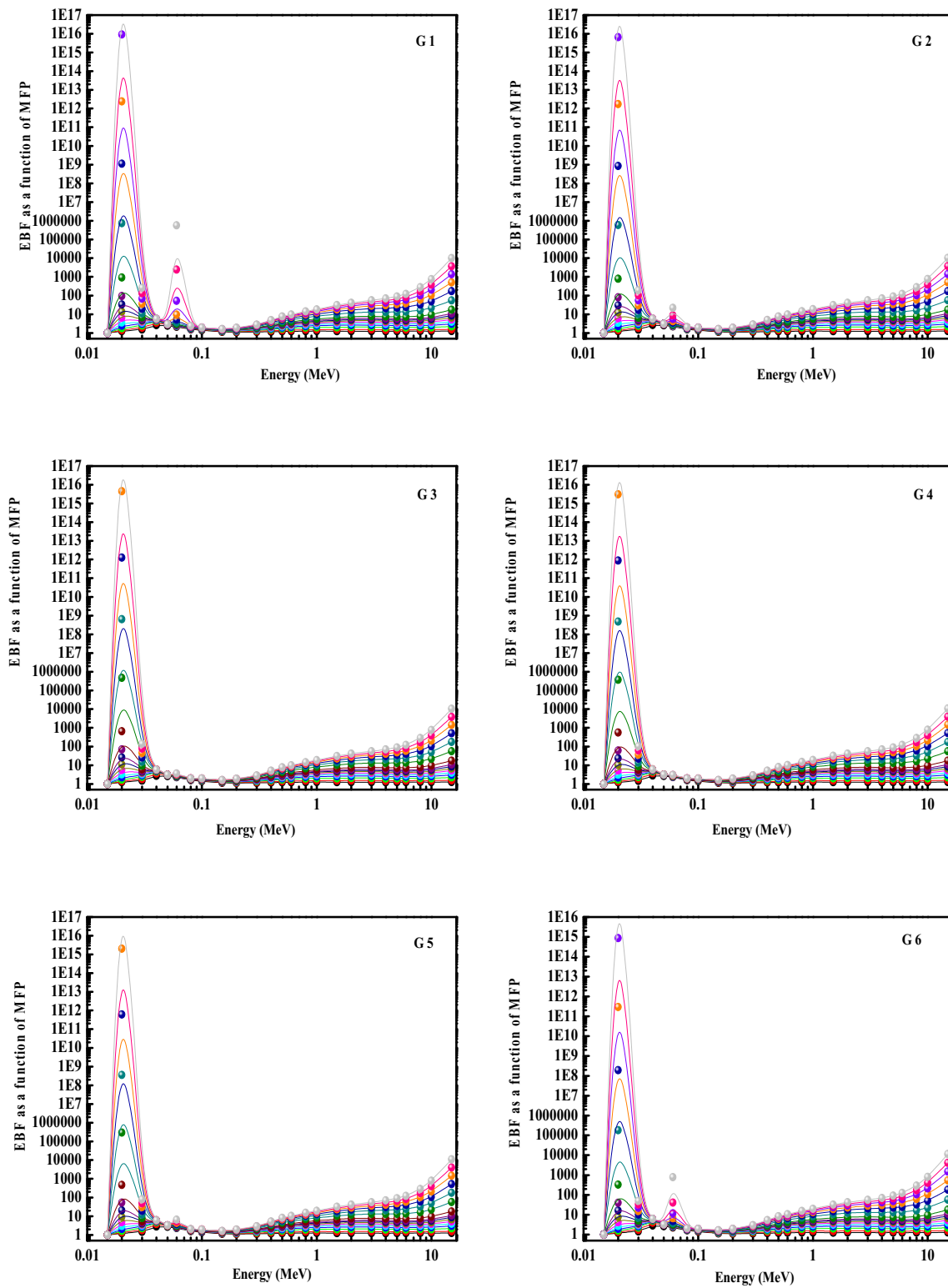


Fig. 14 Variations of the energy absorption build-up factors (EBF) with photon energy for glass samples

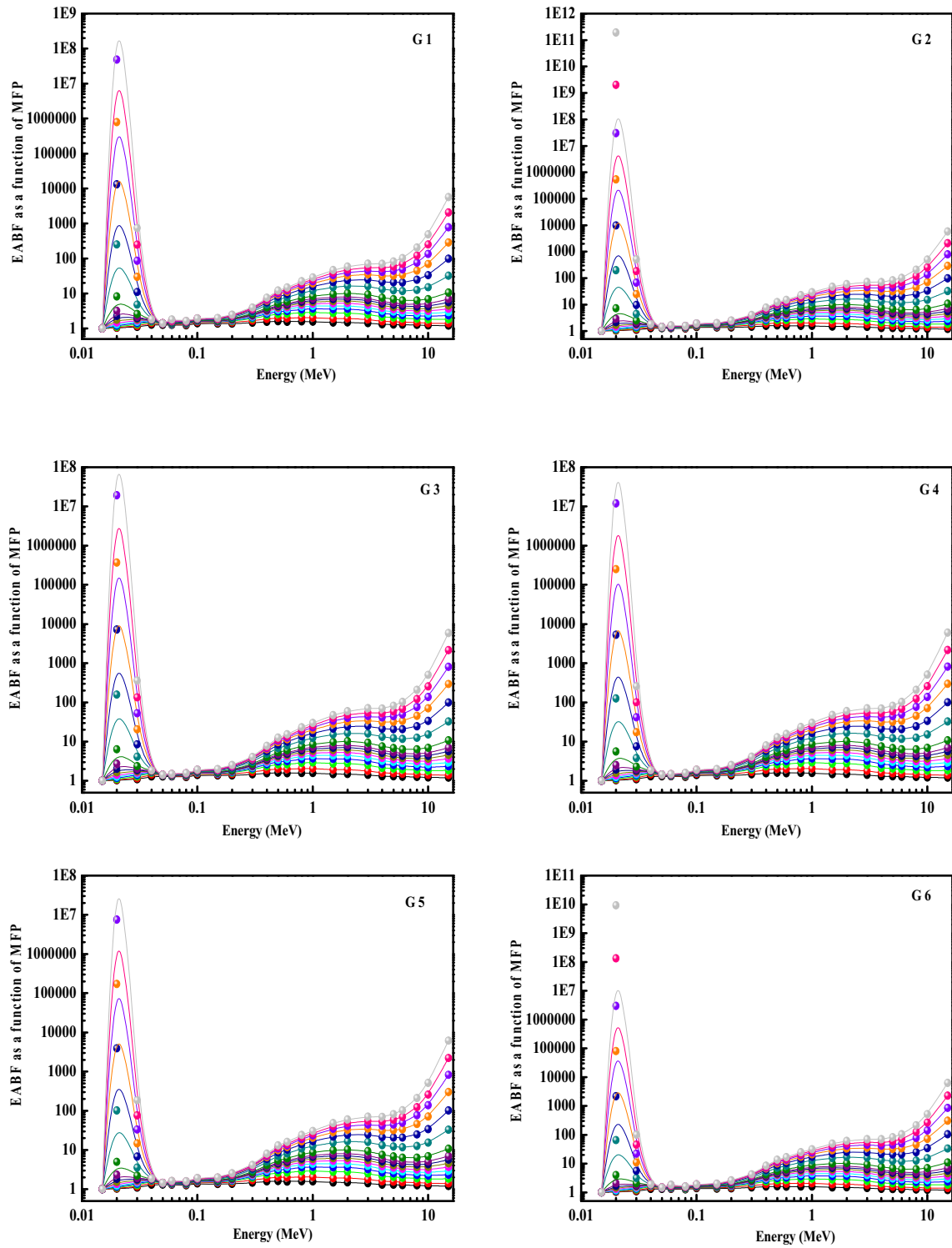


Fig. 15 Variations of the energy absorption build-up factors (EABF) with photon energy for glass samples

Table 8 G-P fitting parameters for EBF and G-P fitting parameters for EABF of glass name G 1

Energy (MeV)	G-P fitting parameters for EBF					G-P fitting parameters for EABF				
	<i>a</i>	<i>b</i>	<i>c</i>	<i>d</i>	<i>Xk</i>	<i>a</i>	<i>b</i>	<i>c</i>	<i>d</i>	<i>Xk</i>
1.50E−02	− 0.430	1.002	1.807	0.301	8.427	− 0.430	1.002	1.807	0.301	8.427
2.00E−02	0.568	1.418	0.612	− 0.784	11.447	0.330	1.064	0.710	− 0.377	14.073
3.00E−02	0.173	1.900	0.605	− 0.107	18.760	0.200	1.184	0.615	− 0.158	16.882
4.00E−02	0.110	3.517	0.323	− 0.041	22.064	0.120	1.423	0.331	− 0.080	23.546
5.00E−02	− 0.258	2.895	0.071	0.035	12.058	− 0.112	1.350	0.084	0.094	8.783
6.00E−02	1.037	2.309	0.031	− 0.147	17.216	0.757	1.311	0.047	− 0.188	14.881
8.00E−02	0.748	1.646	0.047	− 0.251	14.386	0.561	1.298	0.091	− 0.225	14.051
1.00E−01	0.380	1.532	0.124	− 0.071	16.508	0.368	1.533	0.125	− 0.073	15.996
1.50E−01	0.432	1.197	0.181	− 0.241	13.797	0.631	1.453	0.078	− 0.304	13.922
2.00E−01	0.221	1.168	0.404	− 0.117	14.185	0.463	1.493	0.161	− 0.257	13.780
3.00E−01	0.142	1.242	0.548	− 0.065	13.813	0.311	1.675	0.294	− 0.176	13.399
4.00E−01	0.099	1.325	0.671	− 0.053	14.226	0.238	1.887	0.414	− 0.155	13.783
5.00E−01	0.076	1.393	0.743	− 0.045	14.150	0.187	2.020	0.510	− 0.127	13.849
6.00E−01	0.059	1.438	0.797	− 0.036	13.748	0.138	1.967	0.611	− 0.095	13.657
8.00E−01	0.039	1.499	0.867	− 0.028	13.691	0.102	2.047	0.706	− 0.076	13.599
1.00E+00	0.024	1.520	0.923	− 0.023	13.507	0.082	2.052	0.766	− 0.068	13.511
1.50E+00	0.002	1.498	1.026	− 0.017	13.988	0.046	1.909	0.893	− 0.052	13.672
2.00E+00	0.002	1.527	1.043	− 0.021	13.111	0.057	1.941	0.877	− 0.068	13.342
3.00E+00	0.011	1.532	1.035	− 0.038	13.176	0.068	1.804	0.868	− 0.089	13.372
4.00E+00	0.016	1.473	1.034	− 0.045	13.424	0.062	1.586	0.892	− 0.085	13.630
5.00E+00	0.046	1.500	0.952	− 0.072	13.656	0.089	1.562	0.828	− 0.109	13.853
6.00E+00	0.058	1.488	0.927	− 0.082	13.871	0.102	1.513	0.803	− 0.121	14.051
8.00E+00	0.079	1.529	0.890	− 0.098	14.153	0.111	1.479	0.798	− 0.126	14.306
1.00E+01	0.056	1.502	0.981	− 0.077	14.203	0.087	1.414	0.886	− 0.102	14.336
1.50E+01	0.034	1.576	1.131	− 0.059	14.123	0.062	1.407	1.027	− 0.085	14.252

4 Conclusion

The melt-quenching method has been used to fabricate $53\text{B}_2\text{O}_3-2\text{NaF}-27\text{PbO}-(20-x)\text{BaO}-x\text{La}_2\text{O}_3$ ($0 \leq x \leq 15$) glass system. The current glass sample's mechanical and thermal characteristics depend on the glass structure. It is observed that ultrasonic velocities and elastic modulus (experimental and theoretical) for these glasses are increased. FT-IR analysis shows that with the increase of La_2O_3 increases the changes of BO_3 to BO_4 and increases the degree of glass connectivity, and the structural units of $(\text{BO}_3/2\text{F})^-$ tetrahedra are formed. It has been noted that the MAC values of glass samples are

decreased to 1 meV, apart from a small increase at 0.1 meV. At low energy, this significant decline and small peak are directly linked to the current photoelectric effect. It has been noted that the (HVL) and (TVL) increase with the increase in the photon energy and La_2O_3 content rendering to the achieved results. It has been noted that at low energy levels, the EABFs and EBFs originally possess very high values, as the photoelectric effect dominates and replaces the BaO with La_2O_3 .

Table 9 G-P fitting parameters for EBF and G-P fitting parameters for EABF of glass name G 6

Energy (MeV)	G-P fitting parameters for EBF					G-P fitting parameters for EABF				
	<i>a</i>	<i>b</i>	<i>c</i>	<i>d</i>	<i>Xk</i>	<i>a</i>	<i>b</i>	<i>c</i>	<i>d</i>	<i>Xk</i>
1.50E-02	- 0.427	1.002	1.812	0.300	8.485	- 0.427	1.002	1.812	0.300	8.485
2.00E-02	0.608	1.335	0.508	- 0.841	11.310	0.353	1.053	0.612	- 0.404	13.774
3.00E-02	0.178	1.745	0.562	- 0.097	17.567	0.208	1.154	0.572	- 0.161	15.890
4.00E-02	0.088	3.939	0.327	- 0.033	23.386	0.107	1.490	0.325	- 0.045	23.165
5.00E-02	- 0.263	3.143	0.079	0.029	12.398	- 0.115	1.406	0.092	0.089	9.059
6.00E-02	0.932	2.489	0.039	- 0.134	15.628	0.666	1.363	0.058	- 0.154	15.856
8.00E-02	0.777	1.696	0.029	- 0.232	14.647	0.611	1.322	0.070	- 0.228	14.087
1.00E-01	0.485	1.509	0.092	- 0.107	15.741	0.470	1.503	0.094	- 0.108	15.354
1.50E-01	0.413	1.196	0.196	- 0.231	13.782	0.609	1.447	0.086	- 0.300	13.875
2.00E-01	0.214	1.174	0.415	- 0.114	14.189	0.446	1.499	0.173	- 0.250	13.795
3.00E-01	0.139	1.256	0.555	- 0.065	13.819	0.302	1.704	0.306	- 0.171	13.429
4.00E-01	0.096	1.344	0.679	- 0.053	14.204	0.230	1.927	0.429	- 0.150	13.799
5.00E-01	0.073	1.412	0.755	- 0.044	14.140	0.178	2.037	0.531	- 0.121	13.856
6.00E-01	0.055	1.457	0.810	- 0.035	13.760	0.133	2.009	0.626	- 0.093	13.668
8.00E-01	0.036	1.516	0.880	- 0.027	13.686	0.097	2.081	0.720	- 0.074	13.601
1.00E+00	0.022	1.535	0.934	- 0.022	13.489	0.078	2.079	0.780	- 0.066	13.512
1.50E+00	0.000	1.506	1.036	- 0.016	13.913	0.044	1.930	0.899	- 0.052	13.643
2.00E+00	0.002	1.538	1.043	- 0.022	13.099	0.056	1.960	0.880	- 0.067	13.333
3.00E+00	0.010	1.531	1.040	- 0.037	13.141	0.064	1.787	0.878	- 0.086	13.353
4.00E+00	0.016	1.474	1.034	- 0.045	13.423	0.062	1.587	0.893	- 0.085	13.627
5.00E+00	0.046	1.500	0.952	- 0.072	13.657	0.089	1.562	0.828	- 0.110	13.854
6.00E+00	0.058	1.487	0.927	- 0.082	13.874	0.102	1.513	0.803	- 0.121	14.054
8.00E+00	0.078	1.529	0.891	- 0.098	14.154	0.111	1.479	0.799	- 0.126	14.309
1.00E+01	0.056	1.503	0.985	- 0.076	14.201	0.086	1.414	0.889	- 0.102	14.332
1.50E+01	0.033	1.577	1.137	- 0.059	14.105	0.062	1.408	1.032	- 0.086	14.238

Acknowledgements

The authors extend their appreciation to the Deanship of Scientific Research at King Khalid University for funding this work through research groups program under Grant Number R.G.P. 2/93/41.

Compliance with ethical standards

Conflict of interest The authors declare that they have no known competing financial interests or personal relationships that could have appeared to influence the work reported in this paper.

Ethical approval This article does not contain any studies with human participants or animals performed by any of the authors.

Informed consent Informed consent was obtained from all individual participants included in the study.

References

1. W. Shakespeare, Halide glass. *Struct. Chemi. Glasses* (2002). <https://doi.org/10.1016/b978-008043958-7/50019-4>
2. M. Yamane, H. Kawazoe, S. Inoue, K. Maeda, IR transparency of the glass of ZnCl₂-KBr-PbBr₂ system. *Mater. Res. Bull.* **20**(8), 905–911 (1985). [https://doi.org/10.1016/0025-5408\(85\)90073-x](https://doi.org/10.1016/0025-5408(85)90073-x)
3. E.A. Abdel Wahab, A.A. El-Maaref, K.S. Shaaban, J. Börcsök, M. Abdelawwad, Lithium cadmium phosphate glasses doped Sm³⁺ as a host material for near-IR laser applications. *Opt. Mater.* (2020). <https://doi.org/10.1016/j.optmat.2020.110638>
4. K.S. Shaaban, Y.B. Saddeek, M.A. Sayed et al., Mechanical and thermal properties of lead borate glasses containing CaO and NaF. *Silicon* **10**, 1973–1978 (2018). <https://doi.org/10.1007/s12633-017-9709-8>
5. A. Okasha, S.Y. Marzouk, A.H. Hammad, A.M. Abdelghany, Optical character inquest of cobalt containing fluoroborate

- glass. *Optik* **142**, 125–133 (2017). <https://doi.org/10.1016/j.ijleo.2017.05.088>
6. M.S. AlBuriahi, H.H. Hegazy, F. Alresheedi, I.O. Olarinoye, H. Algarni, H.O. Tekin, H.A. Saudi, Effect of CdO addition on photon, electron, and neutron attenuation properties of boro-tellurite glasses. *Ceram. Int.* (2020). <https://doi.org/10.1016/j.ceramint.2020.10.168>
 7. S. Stalin, D.K. Gaikwad, M.S. Al-Buriahi, Ch. Srinivasu, S.A. Ahmed, H.O. Tekin, S. Rahman, Influence of Bi₂O₃/WO₃ substitution on the optical, mechanical, chemical durability and gamma ray shielding properties of lithium-borate glasses. *Ceram. Int.* (2020). <https://doi.org/10.1016/j.ceramint.2020.10.109>
 8. M.S. Al-Buriahi, H.H. Smailly, A. Alalawi et al., Polarizability, optical basicity, and photon attenuation properties of Ag₂O–MoO₃–V₂O₅–TeO₂ glasses: the role of silver oxide. *J. Inorg. Organomet. Polym.* (2020). <https://doi.org/10.1007/s10904-020-01750-z>
 9. M.S. Al-Buriahi, Y.S. Alajerami, A.S. Abouhaswa, A. Alalawi, T. Nutaro, B. Tonguc, Effect of chromium oxide on the physical, optical, and radiation shielding properties of lead sodium borate glasses. *J. Non-Cryst. Solids* **544**, 120171 (2020). <https://doi.org/10.1016/j.jnoncrysol.2020.120171>
 10. A.S. Abouhaswa, M.H.A. Mhareb, A. Alalawi, M.S. Al-Buriahi, Physical, structural, optical, and radiation shielding properties of B₂O₃–20Bi₂O₃–20Na₂O–Sb₂O₃ glasses: role of Sb₂O₃. *J. Non-Cryst. Solids* **543**, 120130 (2020). <https://doi.org/10.1016/j.jnoncrysol.2020.120130>
 11. K.A. Naseer, K. Marimuthu, M.S. Al-Buriahi, A. Alalawi, H.O. Tekin, Influence of Bi₂O₃ concentration on barium-telluro-borate glasses: physical, structural and radiation-shielding properties. *Ceram. Int.* **47**(1), 329–340 (2020). <https://doi.org/10.1016/j.ceramint.2020.08.138>
 12. K.S. Shaaban, E.A.A. Wahab, E.R. Shaaban et al., Electronic polarizability, optical basicity, thermal, mechanical and optical investigations of (65B₂O₃–30Li₂O–5Al₂O₃) glasses doped with titanate. *J. Electron. Mater.* **49**, 2040–2049 (2020). <https://doi.org/10.1007/s11664-019-07889-x>
 13. K.S. Shaaban, S.M. Abo-Naf, M.E.M. Hassouna, Physical and structural properties of lithium borate glasses containing MoO₃. *Silicon* **11**, 2421–2428 (2019). <https://doi.org/10.1007/s12633-016-9519-4>
 14. W.M. Abd-Allah, H.A. Saudi, K.S. Shaaban et al., Investigation of structural and radiation shielding properties of 40B₂O₃–30PbO–(30–x) BaO–x ZnO glass system. *Appl. Phys. A* **125**, 275 (2019). <https://doi.org/10.1007/s00339-019-2574-0>
 15. K.S. Shaaban, S.M. Abo-naf, A.M. Abd Elnaem, M.E.M. Hassouna, Studying effect of MoO₃ on elastic and crystallization behavior of lithium diborate glasses. *Appl. Phys. A* (2017). <https://doi.org/10.1007/s00339-017-1052-9>
 16. E.A.A. Wahab, K.S. Shaaban, Effects of SnO₂ on spectroscopic properties of borosilicate glasses before and after plasma treatment and its mechanical properties. *Mater. Res. Express* **5**(2), 025207 (2018). <https://doi.org/10.1088/2053-1591/aaee8>
 17. R.M. El-Sharkawy, K.S. Shaaban, R. Elsaman, E.A. Allam, A. El-Taher, M.E. Mahmoud, Investigation of mechanical and radiation shielding characteristics of novel glass systems with the composition xNiO–20ZnO–60B₂O₃–(20–x) CdO based on nano metal oxides. *J. Non-Cryst. Solids* **528**, 119754 (2019). <https://doi.org/10.1016/j.jnoncrysol.2019.119754>
 18. K.S. Shaaban, Y. El Sayed, Optical properties of Bi₂O₃ doped boro tellurite glasses and glass ceramics. *Optik* **203**, 163976 (2020). <https://doi.org/10.1016/j.ijleo.2019.163976>
 19. E.A. Abdel Wahab, K.S. Shaaban, R. Elsaman et al., Radiation shielding, and physical properties of lead borate glass doped ZrO₂ nanoparticles. *Appl. Phys. A* **125**, 869 (2019). <https://doi.org/10.1007/s00339-019-3166-8>
 20. I. Boukhris, I. Kebaili, M.S. Al-Buriahi, A. Alalawi, A.S. Abouhaswa, B. Tonguc, Photon and electron attenuation parameters of phosphate and borate bioactive glasses by using Geant4 simulations. *Ceram. Int.* **46**(15), 24435–24442 (2020). <https://doi.org/10.1016/j.ceramint.2020.06.226>
 21. S. Ibrahim, F.H. ElBatal, A.M. Abdelghany, Optical character enrichment of NdF₃ – doped lithium fluoroborate glasses. *J. Non-Cryst. Solids* **453**, 16–22 (2016). <https://doi.org/10.1016/j.jnoncrysol.2016.09.017>
 22. E. Şakar, Ö.F. Özpölat, B. Alım, M.I. Sayyed, M. Kurudirek, Phy-X / PSD: Development of a user-friendly online software for calculation of parameters relevant to radiation shielding and dosimetry. *Radiat. Phys. Chem.* (2020). <https://doi.org/10.1016/j.radphyschem.2019.108496>
 23. K.S. Shaaban, E.A.A. Wahab, E.R. Shaaban et al., Electronic polarizability, optical basicity and mechanical properties of aluminum lead phosphate glasses. *Opt. Quant. Electron.* **52**, 125 (2020). <https://doi.org/10.1007/s11082-020-2191-3>
 24. K.S. Shaaban, E.S. Yousef, S.A. Mahmoud et al., Mechanical, structural and crystallization properties in titanate doped phosphate glasses. *J. Inorg. Organomet. Polym.* (2020). <https://doi.org/10.1007/s10904-020-01574-x>
 25. K.S. Shaaban, M.S.I. Koubisy, H.Y. Zahran et al., Spectroscopic properties, electronic polarizability, and optical basicity of titanium–cadmium tellurite glasses doped with different amounts of lanthanum. *J. Inorg. Organomet. Polym.* (2020). <https://doi.org/10.1007/s10904-020-01640-4>
 26. H.H. Smailly, K.S. Shaaban, S.A. Makhlof et al., Comparative studies on polarizability, optical basicity and optical properties of lead borosilicate modified with titania. *J. Inorg.*

- Organomet. Polym (2020). <https://doi.org/10.1007/s10904-020-01650-2>
27. A. Makishima, J.D. Mackenzie, Direct calculation of Young's modulus of glass. *J. Non-Cryst. Solids* **12**(1), 35–45 (1973). [https://doi.org/10.1016/0022-3093\(73\)90053-7](https://doi.org/10.1016/0022-3093(73)90053-7)
 28. A. Makishima, J.D. Mackenzie, Calculation of bulk modulus, shear modulus, and Poisson's ratio of glass. *J. Non-Cryst. Solids* **17**(2), 147–157 (1975). [https://doi.org/10.1016/0022-3093\(75\)90047-2](https://doi.org/10.1016/0022-3093(75)90047-2)
 29. K. Shaaban, E.A. Abdel Wahab, A.A. El-Maaref et al., Judd-Ofelt analysis and physical properties of erbium modified cadmium lithium gadolinium silicate glasses. *J. Mater. Sci.: Mater. Electron.* **31**, 4986–4996 (2020). <https://doi.org/10.1007/s10854-020-03065-8>
 30. K.S. Shaaban, H.Y. Zahran, I.S. Yahia et al., Mechanical and radiation-shielding properties of B_2O_3 - P_2O_5 - Li_2O - MoO_3 glasses. *Appl. Phys. A* **126**, 804 (2020). <https://doi.org/10.1007/s00339-020-03982-9>
 31. A.M. Fayad, K.S. Shaaban, W.M. Abd-Allah et al., Structural and optical study of CoO doping in borophosphate host glass and effect of gamma irradiation. *J. Inorg. Organomet. Polym.* (2020). <https://doi.org/10.1007/s10904-020-01641-3>
 32. H.A. Saudi, W.M. Abd-Allah, K.S. Shaaban, Investigation of gamma and neutron shielding parameters for borosilicate glasses doped europium oxide for the immobilization of radioactive waste. *J. Mater. Sci.: Mater. Electron.* **31**, 6963–6976 (2020). <https://doi.org/10.1007/s10854-020-03261-6>
 33. K.S. Shaaban, E.S. Yousef, E.A. Abdel Wahab et al., Investigation of crystallization and mechanical characteristics of glass and glass-ceramic with the compositions xFe_2O_3 - $35SiO_2$ - $35B_2O_3$ - $10Al_2O_3$ - $(20-x)Na_2O$. *J. Mater. Eng. Perform* **29**, 4549–4558 (2020). <https://doi.org/10.1007/s11665-020-04969-6>
 34. A.F.A. El-Rehim, A.M. Ali, H.Y. Zahran et al., Spectroscopic, structural, thermal, and mechanical properties of B_2O_3 - CeO_2 - PbO_2 glasses. *J. Inorg. Organomet. Polym.* (2020). <https://doi.org/10.1007/s10904-020-01799-w>
 35. A.A. El-Maaref, E.A.A. Wahab, K.S. Shaaban, M. Abdelawwad, M.S.I. Koubisy, J. Börcsök, E.S. Yousef, Visible and mid-infrared spectral emissions and radiative rates calculations of Tm^{3+} doped BBLC glass. *Spectrochim. Acta A* (2020). <https://doi.org/10.1016/j.saa.2020.118774>
 36. E.A. Abdel Wahab, K.S. Shaaban, E.S. Yousef, Enhancement of optical and mechanical properties of sodium silicate glasses using zirconia. *Opt. Quant. Electron.* **52**, 458 (2020). <https://doi.org/10.1007/s11082-020-02575-3>
 37. E.I. Kamitsos, A.P. Patsis, M.A. Karakassides, G.D. Chrysikos, Infrared reflectance spectra of lithium borate glasses. *J. Non-Cryst. Solids* **126**(1–2), 52–67 (1990). [https://doi.org/10.1016/0022-3093\(90\)91023-k](https://doi.org/10.1016/0022-3093(90)91023-k)
 38. S. Ibrahim, M.M. Gomaa, H. Darwish, Influence of Fe_2O_3 on the physical, structural, and electrical properties of sodium lead borate glasses. *J. Adv. Ceram.* **3**(2), 155–164 (2014). <https://doi.org/10.1007/s40145-014-0107-z>
 39. A.M. Abdelghany, H.A. ElBatal, Optical and μ -FTIR mapping: a new approach for structural evaluation of V_2O_5 -lithium fluoroborate glasses. *Mater. Des.* **89**, 568–572 (2016). <https://doi.org/10.1016/j.matdes.2015.09.159>
 40. A.K. Varshneya, *Fundamentals of Inorganic Glasses* (Academic Press Limited, Boston, 1994), p. 33
 41. M.S. Al-Buriahi, E.M. Bakhsh, B. Tonguc, S. Bahadar Khan, Mechanical and radiation shielding properties of tellurite glasses doped with ZnO and NiO. *Ceram. Int.* (2020). <https://doi.org/10.1016/j.ceramint.2020.04.240>
 42. M.S. Al-Buriahi, B. Tonguç, U. Perişanoğlu, E. Kavaz, The impact of Gd_2O_3 on nuclear safety proficiencies of TeO_2 - ZnO - Nb_2O_5 glasses: a GEANT4 Monte Carlo study. *Ceram. Int.* (2020). <https://doi.org/10.1016/j.ceramint.2020.03.110>
 43. M.S. Al-Buriahi, V.P. Singh, A. Alalawi, C. Sriwunkum, B.T. Tonguc, Mechanical features and radiation shielding properties of TeO_2 - Ag_2O - WO_3 glasses. *Ceram. Int.* (2020). <https://doi.org/10.1016/j.ceramint.2020.03.091>
 44. S. Ozturk, E. Ilik, G. Kilic et al., Ta_2O_5 -doped zinc-borate glasses: physical, structural, optical, thermal, and radiation shielding properties. *Appl. Phys. A* **126**, 844 (2020). <https://doi.org/10.1007/s00339-020-04041-z>
 45. E.A. Abdel Wahab, M.S.I. Koubisy, M.I. Sayyed, K.A. Mahmoud, A.F. Zatssepın, S.A. Makhlof, Kh.S. Shaaban, Novel borosilicate glass system: $Na_2B_4O_7$ - SiO_2 - MnO_2 synthesis, average electronics polarizability, optical basicity, and gamma-ray shielding features. *J. Non-Cryst. Solids* (2020). <https://doi.org/10.1016/j.jnoncrsol.2020.120509>
 46. I. Boukhris, I. Kebaili, M.S. Al-Buriahi et al., Effect of lead oxide on the optical properties and radiation shielding efficiency of antimony-sodium-tungsten glasses. *Appl. Phys. A* **126**, 763 (2020). <https://doi.org/10.1007/s00339-020-03932-5>
 47. M.I. Sayyed, H. Akyildirim, M.S. Al-Buriahi et al., Oxyfluoro-tellurite-zinc glasses and the nuclear-shielding ability under the substitution of AlF_3 by ZnO. *Appl. Phys. A* **126**, 88 (2020). <https://doi.org/10.1007/s00339-019-3265-6>
 48. A.A. El-Rehim, H. Zahran, I. Yahia et al., Radiation, crystallization, and physical properties of cadmium borate glasses. *Silicon* (2020). <https://doi.org/10.1007/s12633-020-00798-3>
 49. Y.S. Rammah, H.O. Tekin, C. Sriwunkum, I. Olarinoye, A. Alalawi, M.S. Al-Buriahi, B.T. Tonguc, Investigations on borate glasses within SBC-Bx system for gamma-ray shielding applications. *Nucl. Eng. Technol.* (2020). <https://doi.org/10.1016/j.net.2020.06.034>

50. I.O. Olarinoye, Y.S. Rammah, S. Alraddadi, C. Sriwunkum, A.F. Abd El-Rehim, H.Y. Zahran, M.S. Al-Buriahi, The effects of La_2O_3 addition on mechanical and nuclear shielding properties for zinc borate glasses in Monte Carlo simulation. *Ceram. Int.* (2020). <https://doi.org/10.1016/j.ceramint.2020.08.092>
51. M.S. Al-Buriahi, C. Sriwunkum, H. Arslan et al., Investigation of barium borate glasses for radiation shielding applications. *Appl. Phys. A* **126**, 68 (2020). <https://doi.org/10.1007/s00339-019-3254-9>
52. M.S. Al-Buriahi, H.O. Tekin, E. Kavaz et al., New transparent rare earth glasses for radiation protection applications. *Appl. Phys. A* **125**, 866 (2019). <https://doi.org/10.1007/s00339-019-3077-8>
53. M.S. Al-Buriahi, B.T. Tonguc, Study on gamma-ray buildup factors of bismuth borate glasses. *Appl. Phys. A* **125**, 482 (2019). <https://doi.org/10.1007/s00339-019-2777-4>
54. M.S. Al-Buriahi, K.S. Mann, Radiation shielding investigations for selected tellurite-based glasses belonging to the TNW system. *Mater. Res. Express* **6**(10), 105206 (2019). <https://doi.org/10.1088/2053-1591/ab3f85>
55. E.A. Abdel Wahab, M.S.I. Koubisy, M.I. Sayyed, K.A. Mahmoud, A.F. Zatsopin, S.A. Makhlof, Kh.S. Shaaban, Novel borosilicate glass system: $\text{Na}_2\text{B}_4\text{O}_7\text{-SiO}_2\text{-MnO}_2$: synthesis, average electronics polarizability, optical basicity, and gamma-ray shielding features. *J. Non-Cryst. Solids* (2020). <https://doi.org/10.1016/j.jnoncrysol.2020.120509>
56. M.S. Al-Buriahi, A.S. Abouhaswa, H.O. Tekin, C. Sriwunkum, F.I. El-Agawany, T. Nutaro, E. Kavaz, Y.S. Rammah, Structure, optical, gamma-ray and neutron shielding properties of NiO doped $\text{B}_2\text{O}_3\text{-BaCO}_3\text{-Li}_2\text{O}_3$ glass systems. *Ceram. Int.* **46**(2), 1711–1721 (2020). <https://doi.org/10.1016/j.ceramint.2019.09.144>

Publisher's Note Springer Nature remains neutral with regard to jurisdictional claims in published maps and institutional affiliations.